Available online at www.sciencedirect.com
ScienceDirect
Solid State Ionics 178 (2008) 1950–1957
SOLID STATE IONICS
www.elsevier.com/locate/ssi

Refinement of the bulk defect model for $La_xSr_{1-x}MnO_{3\pm\delta}$ ☆

David S. Mebane [a,1], Yingjie Liu [b,2], Meilin Liu [a,*]

[a] School of Materials Science and Engineering, Georgia Institute of Technology, United States
[b] School of Mathematics, Georgia Institute of Technology, United States

Received 13 April 2007; received in revised form 1 January 2008; accepted 4 January 2008

Abstract

The literature nonstoichiometry data for bulk defects in $La_xSr_{1-x}MnO_{3\pm\delta}$ (LSM) has been analyzed using a rigorous inverse-problem methodology. A solver–optimizer combination of Newton's method and the particle swarm optimizer (PSO) was developed, along with a rigorous method for determining local identifiability in the comparison between defect models and experimental data. It was found that previous models, which do not account for any excess free energy for defects, cannot adequately replicate nonstoichiometry data at low temperatures. A revised model is proposed that includes excess free energy due to strain field interaction between cation defects. The revised model was shown to be consistently distinguishable from the earlier model (a better fit) even when using a model structure containing fewer parameters. It was also identifiable for 10 and 20% Sr-doping. Data for activation energies and vibrational entropy for the various defect reactions was compiled.

Keywords: LSM; Defects; Nonstoichiometry; Strain field interaction; Inverse problem; Identifiability; Particle swarm

1. Introduction

At Georgia Tech, we have initiated a thorough, quantitative study of oxygen reduction on $La_xSr_{1-x}MnO_{3\pm\delta}$ (LSM) [1–4]. The principal technique of the program is the application of phenomenological models to carefully designed electrochemical test cells. The model and test cell are compared using rigorous inverse problem techniques, producing both qualitative assessment of models and quantitative estimation of parameters. Similar efforts for platinum electrodes on Y_2O_3-doped ZrO_2 (YSZ) have been initiated by Mitterdorfer and Gauckler [5–7], by Bieberle and Gauckler [8] and Bessler [9] for nickel electrodes on YSZ, and by Baumann et al. [10] for $La_xSr_{1-x}Co_yFe_{1-y}O_{3-\delta}$ (LSCF). LSM presents a particular challenge because of the complexity of its behavior with respect to oxygen reduction; however, it is a challenge that must be met in light of the material's continued dominance in solid oxide fuel cell applications.

We propose to address the problem by designing and fabricating test cells with precisely controlled geometries, isolating various material behaviors. Toward this goal, one of the first challenges is an accurate understanding of the bulk defect structure, experimentally accessible through gravimetry and wet chemical methods (such as iodometry), and directly observable through TEM and neutron diffraction. The principal difficulty is that oxygen defects, which are crucial to LSM's behavior as a mixed ionic–electronic conductor, are very rare in LSM at near-atmospheric partial pressures of oxygen and low cathodic overpotentials. This means that direct measurement of the oxygen defect concentration at near-atmospheric pressures is extremely difficult if even possible. At present, it can only be calculated through a thermodynamic model.

Development of such a model for LSM is now decades old. The principal tool in its development is the nonstoichiometry experiment, wherein a powder sample on a precision balance is brought to a certain temperature and exposed to various partial pressures of oxygen. The weight change can be converted into changes in the oxygen stoichiometry. Early measurements by Kamata [11] were followed by a more in-depth study by Kuo and Anderson [12]. Since then, several authors have made additional measurements (a difficult undertaking, especially for the very low

☆ This work was supported by the Department of Energy, Basic Energy Science, Grant No. DE-FG02-06ER15837.
* Corresponding author.
E-mail addresses: mebane@gatech.edu (D.S. Mebane), yingjie@math.gatech.edu (Y. Liu), meilin.liu@mse.gatech.edu (M. Liu).
[1] Additional support provided by the Boeing Company, through a Boeing Fellowship.
[2] Support provided by the National Science Foundation, Grant No. DMS-0511815.

0167-2738/$ - see front matter © 2008 Elsevier B.V. All rights reserved.
doi:10.1016/j.ssi.2008.01.016

oxygen pressures required to obtain significant oxygen deficiency in LSM) or contributed analysis of the data [13–21].

Poulsen [20] devised a flexible random defects model that can be viewed as the culmination of years of experimental observation and theoretical development by various authors, and applied it to Kuo and Anderson's nonstoichiometry data as well as conductivity data [22]. The ability of the model to replicate nonstoichiometry data was very good, while the fit to conductivity data was less successful.

Our initial goal was to use Poulsen's model straightforwardly to estimate defect reaction equilibrium constants at temperatures and compositions of interest to us, while perhaps improving somewhat on Poulsen's mathematical solution technique in order to obtain a more accurate and verifiable parameter estimate. However, we found that a completely random model inadequately described the behavior of the samples at low-temperatures. This led us to modify the random theory slightly, in order to account for defect self-strain interactions in the cation sublattice. We subjected the new model to a rigorous test with respect to the nonstoichiometry data for LSM20 and LSM10, the result of which supports the hypothesis of the strain model as a better alternative to the random model at low temperatures. With respect to conductivity data, however, the results are still inconclusive.

2. Inverse problem techniques

2.1. Particle swarm optimizer

One of the most important aspects of estimating unknown parameters is the optimization method. We sought a robust optimizer, proven effective in finding global optima in a complex, multi-dimensional search space. Non-gradient methods such as evolutionary and genetic algorithms are the best candidates, and of these perhaps the best (and simplest) is the particle swarm optimizer (PSO).

The PSO was first devised by behavioral scientists to model the flocking behavior of birds, but the inventors quickly realized that they had found a powerful method of computational optimization [23]. The basic principle is that a number of agents, each occupying a point in parameter space, explore the space with a stochastic motion. The velocity of each agent is influenced by the most optimal positions found by its neighbors. Using the method (and notation) of Mendes et al. [24], the process of updating the position of each agent at each iteration may be written:

$$\phi_k = U\left[0, \frac{\phi_{\max}}{||\mathcal{N}||}\right] \quad \forall k \in \mathcal{N} \tag{1a}$$

$$\vec{P}_m = \frac{\sum_k \phi_k \vec{P}_k}{\sum_k \phi_k} \tag{1b}$$

$$\vec{v}_{t+1} = \chi\left[\vec{v}_t + \left(\vec{P}_m - \vec{X}_t\right)\sum_k \phi_k\right] \tag{1c}$$

$$\vec{X}_{t+1} = \vec{X}_t + \vec{v}_{t+1} \tag{1d}$$

where $\mathcal{N}$ is the set of all agents in the neighborhood of the agent being updated, $U[a, b]$ is an operator returning a random number between a and b, $\vec{P}_k$ is the best position found by agent k, $\vec{v}$ is velocity and $\vec{X}$ position. X and $\phi_{\max}$ are constants that must take particular values in order to encourage convergence [25].

Mendes et al. [24] introduced the idea of using the best positions of all the agents in a predetermined neighborhood in the update process (instead of merely the most optimal agent of the neighborhood) and also tested several different neighborhood topologies. The most reliable topology for a series of test problems was what Mendes called the "unselfed ring," wherein an agent's neighborhood consists of its two nearest neighbors, but not itself. This is the topology we used in the following analysis.

2.2. Identification

In parameter estimation exercises, care must be taken to ensure that results are unique. That is, one must ensure that the optimum does not occur at a saddle point. For linear problems, there may be methods to determine global identifiability of a model *a priori*. However, for nonlinear problems of the type we are likely to encounter, it is only possible to examine local identifiability *a posteriori*.

The method we chose is an analysis of the behavior of each individual misfit, or the difference between each data point and the corresponding model output, with respect to changes in the parameters [26]. (The sum of the squares of the misfits is the cost, or the function to be optimized.) One computes a rectangular matrix J via the following

$$\eta : \mathbb{R}^P \rightarrow \mathbb{R}^N \quad N > P \tag{2a}$$

$$J(\alpha) = \nabla\eta(\alpha) \tag{2b}$$

where η is the mapping from parameter space into the output space represented by the model, P is the number of parameters, N is the number of output data points, and α is the optimum parameter set. We compute partial derivatives by finite difference, using a highly accurate algorithm involving complex numbers [27]. The matrix J has dimensions $N \times P$. The test for local identifiability at α is whether the columns of J are linearly independent.

Here we encounter the problem that, due to computational errors, we will never find a truly linearly dependent set of vectors. Perhaps more importantly, it may be that a model, while technically yielding a unique parameter estimate, is nonetheless extremely insensitive to one or more parameters. We must therefore devise a method for analyzing the proximity to linear dependence of this vector set, along with standards to apply to the results. The method we developed can be viewed as a constrained minimization:

$$\min ||Jx||^2 \tag{3a}$$

$$||x||^2 = \beta \quad \beta > 0 \tag{3b}$$

Solving with Lagrange multipliers,

$$J^T Jx + \lambda x = 0 \tag{4a}$$

$$x^T x = \beta$$

$$\Rightarrow x^T J^T Jx = -\lambda x^T x = -\lambda\beta \tag{4b}$$

So the size of the eigenvalue indicates the proximity of the corresponding eigenvector x to the nullspace of J, with the lowest eigenvalue corresponding to the direction in parameter space x along which there is the least change in the cost function.

A more rigorous proof:

$$||\eta(\alpha + sx) - \eta(\alpha)|| = sJx + \mathcal{O}(s^2) \tag{5a}$$

with $||x|| = 1$ and s a scalar. Therefore,

$$||\eta(\alpha + sx) - \eta(\alpha)||^2 = s^2 x^T J^T Jx + \mathcal{O}(s^3) \tag{5b}$$

Let λ_i and r_i, $i \in [1, P]$ be the eigenvalues and eigenvectors, respectively, of $J^T J$. Since $J^T J$ is symmetric, r_i is an orthonormal set. Therefore

$$x = \sum_i c_i r_i \tag{5c}$$

$$x^T J^T Jx = \sum_i c_i^2 \lambda_i \geq \lambda_0 \tag{5d}$$

with λ_0 the smallest eigenvalue. Therefore, by (5b), for any fixed perturbation which is small enough, $||\eta(\alpha + sx) - \eta(\alpha)||$ finds a minimum at $x = r_0$.

With the direction of least change identified, we may easily produce a cost contour along this direction. A qualitative decision may then be made regarding the uniqueness of the fit.

3. Random model

3.1. Model review

Following Poulsen [20], the random defect model is

$$\text{Schottky} : \text{nil} \rightleftharpoons 3V_O^{\cdot\cdot} + V_B'''' + V_A''' \tag{6a}$$

$$\text{Reduction} : \frac{1}{2}O_2(g) + 2\text{Mn}_B^x + \text{V}_O^{\cdot\cdot} \rightleftharpoons \text{O}_O^x + 2\text{Mn}_B^{\cdot} \tag{6b}$$

$$\text{Disproportionation} : 2\text{Mn}_B^x \rightleftharpoons \text{Mn}_B^{'} + \text{Mn}_B^{\cdot} \tag{6c}$$

where $\text{V}_O^{\cdot\cdot}$ is an oxygen vacancy with effective 2+ charge, V_B'''' and V_A''' are B- and A-site vacancies, respectively, each carrying an effective 3− charge, Mn_B', Mn_B^X and $\text{Mn}_B^{\cdot}$ are manganese (II), (III) and (IV), respectively, on the B-site and O_O^x denotes an oxygen on an oxygen site. Assuming a random distribution over limited sites in reactions (6b) and (6c), and unlimited sites in (6a), we write the following mass-action laws:

$$K_s = [\text{V}_A'''][\text{V}_B''''][\text{V}_O^{\cdot\cdot}]^3 \tag{7a}$$

$$K_r = \frac{[\text{Mn}_B^{\cdot}]^2(1 - [\text{V}_O^{\cdot\cdot}])}{(1 - [\text{Mn}_B^{\cdot}] - [\text{Mn}_B'] - [\text{V}_B''''])^2[V_O^{\cdot\cdot}]pO_2^{1/2}} \tag{7b}$$

$$K_d = \frac{[\text{Mn}_B'][\text{Mn}_B^{\cdot}]}{(1 - [\text{Mn}_B^{\cdot}] - [\text{Mn}_B'] - [\text{V}_B''''])^2} \tag{7c}$$

$$r_A = \frac{1 - [\text{Sr}_A'] - [\text{V}_A''']}{[\text{Sr}_A']} \tag{7d}$$

$$r_B = \frac{1 - [\text{V}_A''']}{1 - [\text{V}_B''']} \tag{7e}$$

$$0 = 6[\text{V}_O^{\cdot\cdot}] + [\text{Mn}_B^{\cdot}] - 3[\text{V}_{(A)}'''] - 3[\text{V}_B''''] - [\text{Sr}_A'] - [\text{Mn}_B'] \tag{7f}$$

where r_A and r_B are the cation ratios of La to Sr and total A-site cations to Mn, respectively. The mass-action expressions are a direct result of the equilibrium of the defect reactions in terms of chemical potentials of the reactants, taking site restrictions into account and assuming no defect interaction (random distribution). Given the equilibrium constants and cation ratios, this is a system of 6 equations and 6 unknowns. Poulsen solved the system using a searching procedure based on a range of possible values for $[\text{V}_O^{\cdot\cdot}]$. We augmented this method by using a Newton solver to find the final solution, using the best result from Poulsen's searching procedure as an initial guess.

3.2. Data selection

In this work we have used nonstoichiometry data gathered by Mizusaki, *et al.* [18]. One reason for this is that we are interested in relatively low temperatures, and Mizusaki's experiments covered a temperature range of interest, from 873 to 1273 K. Another reason is that Mizusaki corrected for the changes in the buoyancy of the atmosphere by subtracting the weight change of

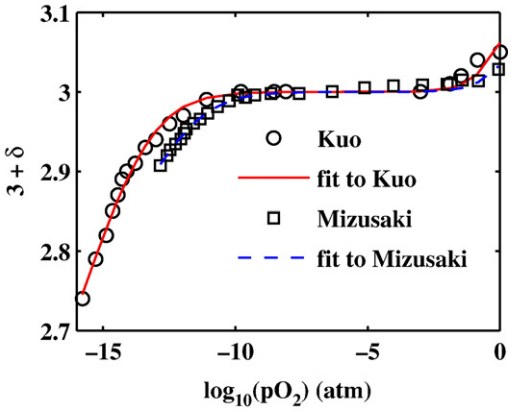

Fig. 1. The fit of the random model to Mizusaki's measurements and Kuo's for $La_{0.8}Sr_{0.2}MnO_{3\pm\delta}$ at 1273 K.

an alumina sample subjected to the same atmosphere and temperature. This approach seems to make a significant difference, as there is a noticeable divergence between Kuo's results and Mizusaki's at 1273 K (the only temperature for which the two overlap), especially at low oxygen pressures. The best fit of Poulsen's model to Mizusaki's data for 20% **Sr**-doping is almost five times better (per data point) than the best fit of the same model to Kuo's measurements at the same composition and temperature (see Fig. 1).

3.3. Fit to low-temperature data

Fits of the random model to Mizusaki's data for $La_{0.8}Sr_{0.2}MnO_{3\pm\delta}$ (LSM20) are found in Fig. 2, and those for $La_{0.9}Sr_{0.1}MnO_{3\pm\delta}$ (LSM10) are found in Fig. 3. The fit to low-pressure data is generally quite good, except at 873 K. At high pressures, however, the experimental data are not captured by the model very well, with an increasing separation as temperature decreases: the experimental increase in stoichiometry is suppressed compared to that of the model. At 873 K, the model completely fails to replicate the data, even at the low-pressure end.

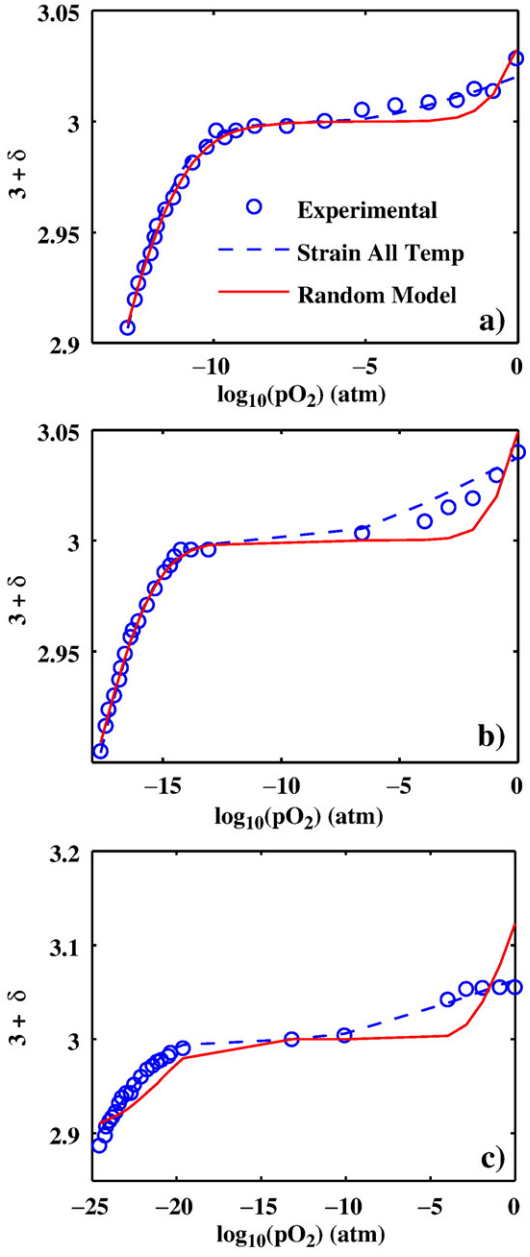

Fig. 2. Fits of both random and strain models to experimental data of ref. [18] for LSM20, at (a) 1273 K (b) 1073 K and (c) 873 K.

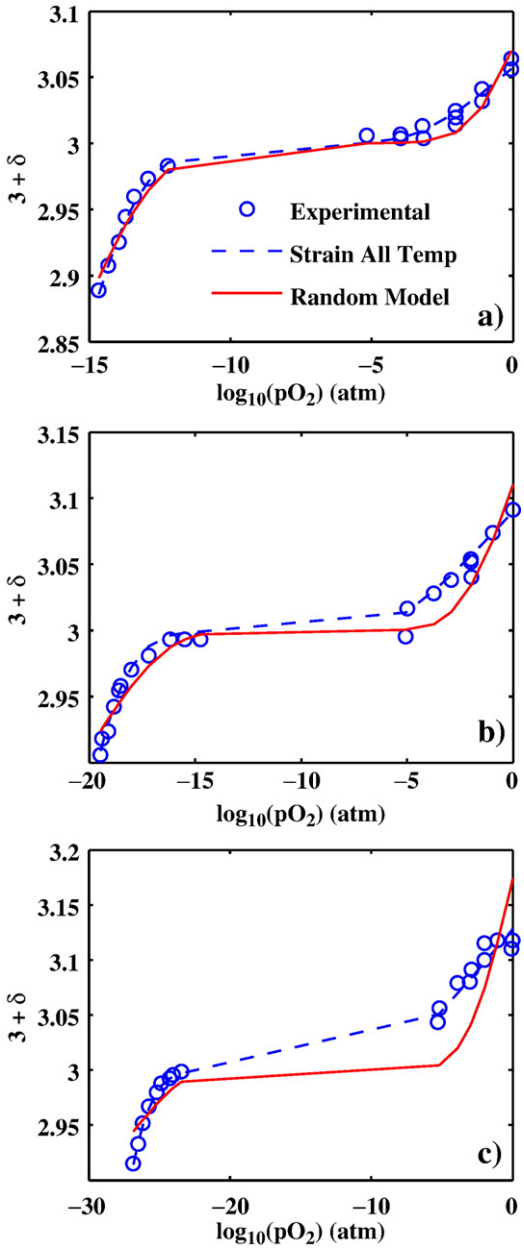

Fig. 3. Fits of both random and strain models to experimental data of ref. [18] for LSM10, at (a) 1273 K (b) 1073 K and (c) 873 K.

4. Strain model

4.1. Rationale and derivation

The suppression of oxygen stoichiometry at high-pressures and low temperatures was pointed out by Mizusaki [18]. It was

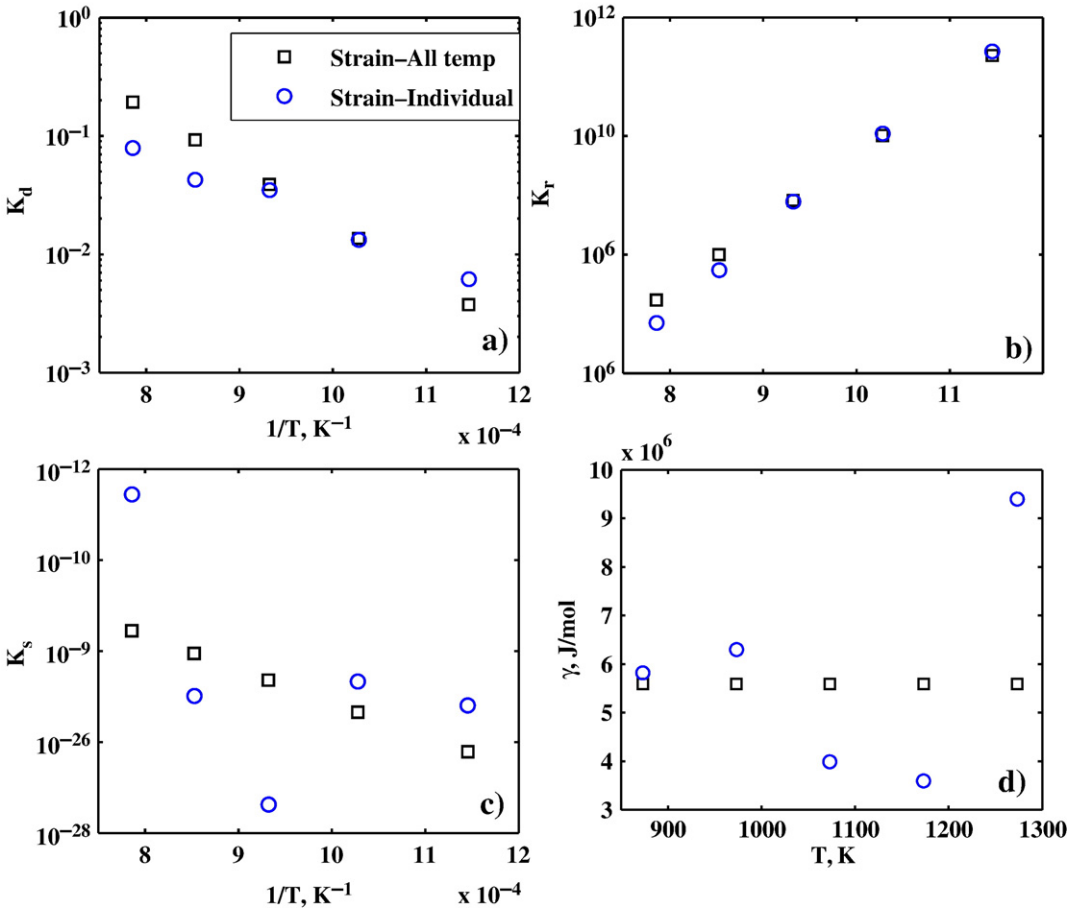

Fig. 4. Parameters found by fitting the strain model to data for LSM20 at each temperature individually, and for all temperatures together. The parameters are (a) κ_d (disproportionation) (b) κ_r (reduction) (c) κ_s (Schottky) (d) γ (strain coefficient).

also clearly reflected in the data of vanRoosmalen and Cordfunke for samples with zero **Sr** content [15]. Since oxygen is added to the crystal past the stoichiometric point through the creation of new sites via the Schottky reaction, the most immediate possibility is a repulsive interaction between vacancies which tends to shift reaction (6a) toward the perfect crystal. While it is easy to imagine self-stress due to both oxygen and cation vacancies, we concentrated on the cations, since they carry a higher effective charge in Poulsen's model and they are much more plentiful than oxygen vacancies at high pressures [20].

This repulsive interaction can be quantified as a mean-field interaction involving strain fields. The excess free energy due to strain field interaction between crystal defects is quadratic in the concentration of the defect, leading to an excess term in the chemical potential proportional to the concentration [28].[3] Considering vacancies on the A and B sites to be the only defects for which the strain effect is considerable, and further assuming an equal strain due to each type of cation vacancy, leads to a rewriting of the mass-action law for Schottky equilibrium:

$$K_s \exp\left[\frac{-\gamma([V_A'''] + [V_B'''])}{RT}\right] = [V_A'''][V_B'''][V_O^{\cdot\cdot}]^3 \quad (8)$$

where γ is a constant depending on the elastic properties of the material and the amount of strain imparted by each new defect.

4.2. Comparison with experiment and discussion

The basic solution methodology remains the same for the strain model as for the random model—a search through candidate values for $[V_O^{\cdot\cdot}]$ followed by Newton's method.

Initially we fit the model to the data set at each individual temperature, producing Arrhenius plots to determine activation energies and vibrational entropy. We also plotted the strain parameter γ vs. temperature (see Fig. 4). Notably, while the estimated constants for reduction and disproportionation reflect the expected Arrhenius behavior, the data for Schottky equilibrium and strain interaction are erratic.

A look at the local identifiability for these fits revealed the likely culprit for the erratic behavior in the Schottky equilibrium constant: it is by far the least sensitive of all the parameters in the area of the

[3] In particular, see Eqs. (8) and (13) in ref. [28], which specify expressions for strain and stress in terms of concentration of the stress-inducing species. The derivation assumes that the induced strain is constant under compositional changes; we inherit this assumption.

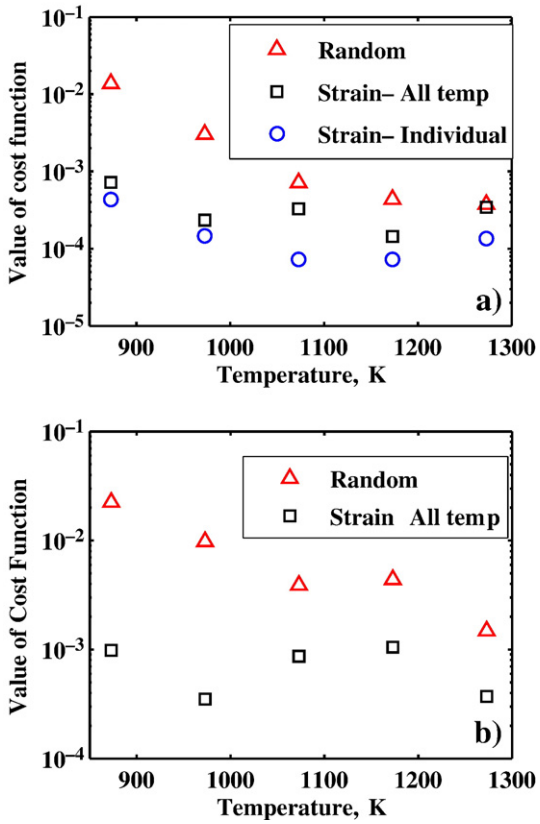

Fig. 5. Comparison of cost values for the fit to data of ref. [18] using the random model fit at each individual temperature and the strain model fit to all temperatures simultaneously for (a) LSM20 and (b) LSM10. For comparison, the fit of the strain model to individual temperatures for LSM20 is shown in part (a).

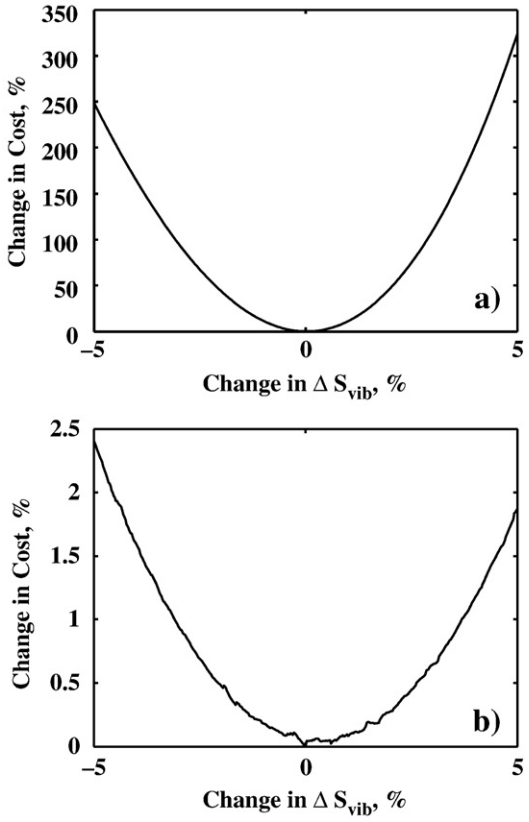

Fig. 6. The change in the cost along the least sensitive direction, with respect to the least sensitive parameter for all-temperature strain model fits to (a) LSM20 and (b) LSM10 data from ref. [18].

optimum at each temperature. The identifiability analysis described in Section 2.2 reveals that at 1273 K, κ_s may change more than 5% while the cost function changes less than 0.01%.[4]

This means that the data gathered in a single nonstoichiometry experiment (at a single temperature) are likely insufficient to uniquely determine the constants in this model.

We may solve this problem, however, if we take advantage of the power of the optimizer to fit this model to all of the temperatures at once. We do this by using the activation energy and vibrational entropy for each defect reaction as parameters, and by requiring the values for γ to be constant across the temperature range. This reduces the ratio of parameters to data points significantly. Additionally, the result of this all-temperature fitting is very useful in comparing the strain model with the random model, since the number of parameters in the fitting is less than the number of parameters used in the random model when fit to each individual temperature at 1273, 1173, 1073, 973 and 873 K. If the strain model is still a quantifiably better fit to the data, we can say that it has passed a significant test.

In fact, the all-temperature fitting of the strain model is consistently better than the fit of the random model at individual temperatures, in terms of the overall value of the cost function at each temperature, for both LSM20 and LSM10 (see Fig. 5). As anticipated, the difference between the models decreases as temperatures increase. The actual fits for selected temperatures are shown in Figs. 2 and 3, while the relevant equilibrium constants and strain parameter for the all-temperature fitting appear in Fig. 4.

The uniqueness behavior is much more stable for LSM20 than the corresponding temperature-by-temperature fit. Fig. 6a shows a plot of the change in the least sensitive parameter (the vibrational entropy of the reduction reaction) along the least sensitive direction in parameter space at the optimum. As reflected in Fig. 6b, there is much less stability in uniqueness behavior for LSM10, with the least sensitive parameter the vibrational entropy for disproportionation. This could suggest that disproportionation is less important for LSM10, however there is also a significant uncertainty in the experimental data for LSM10 which could explain this result. In any event, we regard the uniqueness behavior for LSM10 as good enough to support the results in Fig. 5b.

Table 1
Parameters for LSM20

	κ_d	κ_r	κ_s
ΔH^0, eV	0.944	−2.27	1.46
ΔS^0_{Vib}, kJ/mol·K	57.9	−33.9	−340

[4] The random model suffers from a similar lack of sensitivity in the Schottky equilibrium constant when fit to the data at 1273 K.

Table 2
Parameters for LSM10

	κ_d	κ_r	κ_s
ΔH^0, eV	−0.0057	−3.48	5.64
ΔS^0_{Vib}, kJ/mol·K	−5.76	−106	−45.9

Table 1 lists the optimized activation energies and entropies for LSM20, while Table 2 lists the same parameters for LSM10. Reduction and Schottky activation energies both show a stronger tendency toward the perfect crystal in LSM10, which is reasonable and qualitatively similar to the results of Nowotny and Rekas, who fit a random model to Kuo's data [19]. The disproportionation activation energy tends only slightly toward manganese (III) in LSM20 and is close to zero in LSM10. Lower activation energies for the purely electronic process may be regarded as reasonable given the electronic conductivity of LSM.

The strain interaction parameter, γ, for LSM20 is equal to 5.59×10^6 J/mol·K, and for LSM10 2.17×10^6 J/mol·K.

Defect Kröger–Vink diagrams for both compositions appear in Figs. 7–8.

We tried to use the defect concentrations predicted by the model to fit conductivity data, also gathered by Mizusaki [29]. This exercise was not conclusive. We used a hopping conduction formalism similar to that used by Poulsen [20], but we were not able to fit the mobilities for oxygen vacancies, **Mn(II)** and **Mn (IV)** to the data for LSM20 over the entire data range for either

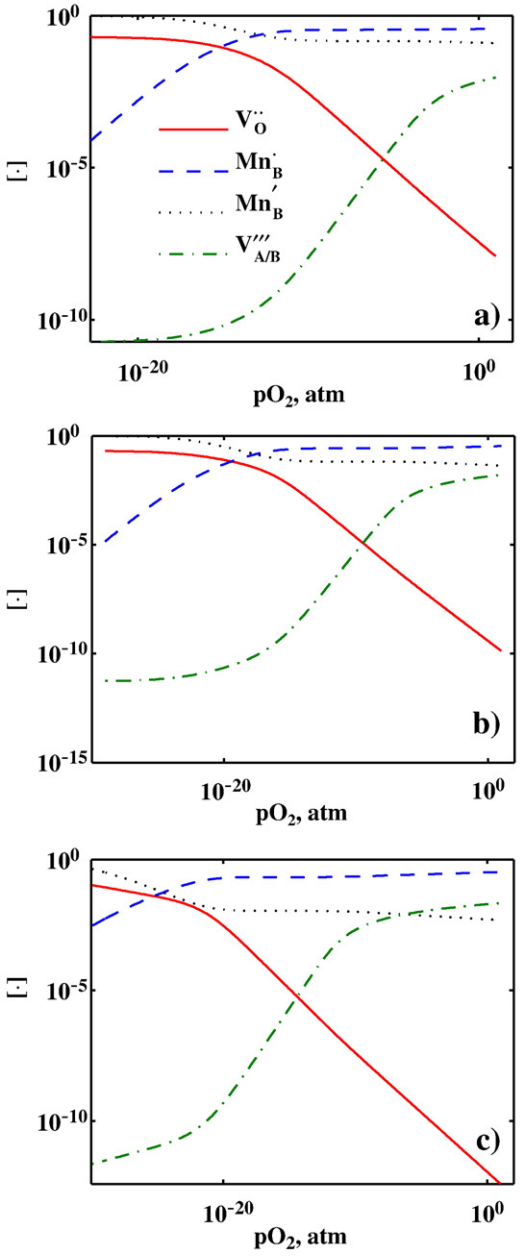

Fig. 7. Kröger–Vink defect diagrams for LSM20, at (a) 1273 K (b) 1073 K and (c) 873 K.

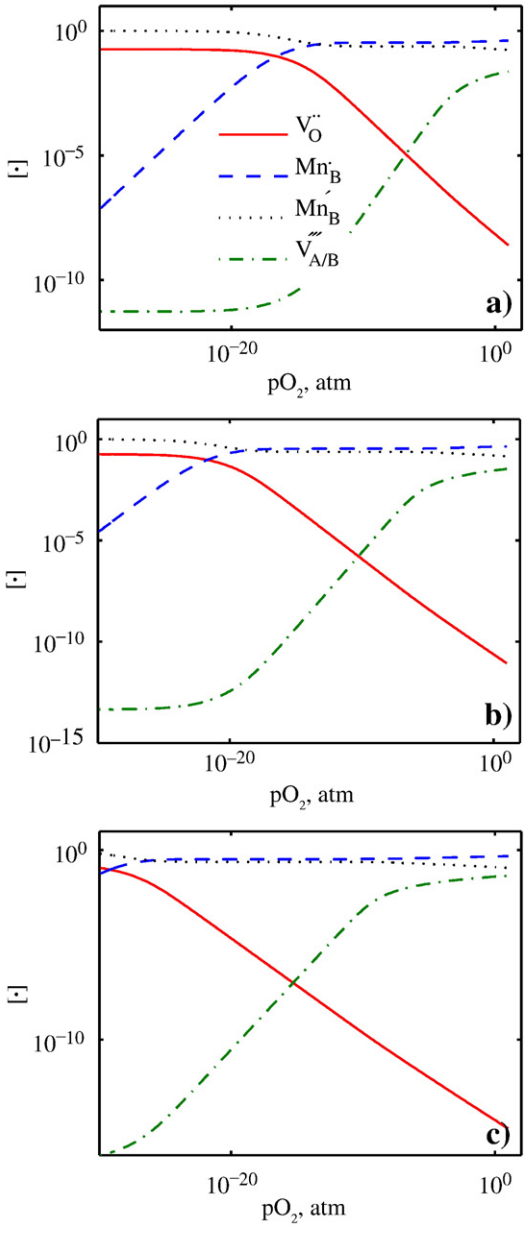

Fig. 8. Kröger–Vink defect diagrams for LSM10, at (a) 1273 K (b) 1073 K and (c) 873 K.

the random or strain models without using a negative mobility for vacancies. The issue is not the leveling out of conductivity at high pressures, which for both random and strain models can be replicated by the proper balance of mobilities for **Mn(II)** and **Mn(IV)**, rather the drop in conductivity as pressures decrease is faster in the experimental data than the drop in concentration of mobile charged species for either model. Further analysis of this data requires a theory of charged species mobility that is related to the defect chemistry in LSM.

5. Conclusion

A robust method of comparing experimental data with phenomenological models for the estimation of model parameters was developed and applied successfully to the estimation of parameters for bulk defect models. The inverse problem method involves the particle swarm optimizer and an analytical method for the assessment of uniqueness. Application to nonstoichiometry data finds that random defect models cannot replicate the experimental data at low temperatures and high pressures in LSM20 and LSM10. A model based on the interaction of strain fields between cation defects was derived and applied to the data set, and it consistently performed better than the random model even when less parameters were used overall in the fitting. The uniqueness of the fits was satisfactory when data at all temperatures were fit at once. These results support the strain model hypothesis.

References

[1] E. Koep, W. Rauch, Z. Zhou, M.L. Liu, Solid State Ionic Devices, Vol. 2002–26 of Proceedings of the Electrochemical Society, The Electrochemical Society, Pennington, NJ, 2002, p. 319.
[2] E. Koep, D.S. Mebane, R. Das, C. Compson, M.L. Liu, Electrochemical and Solid State Letters 8 (11) (2005) A592.
[3] D.S. Mebane, M.L. Liu, Journal of Solid State Electrochemistry 10 (8) (2006) 575.
[4] D.S. Mebane, Y. Liu, M. Liu, Journal of the Electrochemical Society 154 (5) (2007) A421.
[5] A. Mitterdorfer, L.J. Gauckler, Solid State Ionics 120 (1–4) (1999) 211.
[6] A. Mitterdorfer, L.J. Gauckler, Solid State Ionics 117 (3–4) (1999) 187.
[7] A. Mitterdorfer, L.J. Gauckler, Solid State Ionics 117 (3–4) (1999) 203.
[8] A. Bieberle, L.J. Gauckler, Solid State Ionics 146 (1–2) (2002) 23.
[9] W.G. Bessler, Solid State Ionics 176 (11–12) (2005) 997.
[10] F.S. Baumann, J. Fleig, H.U. Habermeier, J. Maier, Solid State Ionics 177 (11–12) (2006) 1071.
[11] K. Kamata, T. Nakajima, T. Hayashi, T. Nakamura, Materials Research Bulletin 13 (1) (1978) 49.
[12] J.H. Kuo, H.U. Anderson, D.M. Sparlin, Journal of Solid State Chemistry 83 (1) (1989) 52.
[13] B.A. vanHassel, T. Kawada, N. Sakai, H. Yokokawa, M. Dokiya, H.J.M. Bouwmeester, Solid State Ionics 66 (1993) 295.
[14] J.A.M. vanRoosmalen, E.H.P. Cordfunke, R.B. Helmholdt, H.W. Zandbergen, Journal of Solid State Chemistry 110 (1) (1994) 100.
[15] J.A.M. vanRoosmalen, E.H.P. Cordfunke, Journal of Solid State Chemistry 110 (1994) 109.
[16] J.A.M. vanRoosmalen, E.H.P. Cordfunke, Journal of Solid State Chemistry 110 (1) (1994) 113.
[17] J. Mizusaki, H. Tagawa, K. Naraya, T. Sasamoto, Solid State Ionics 49 (1991) 111.
[18] J. Mizusaki, N. Mori, H. Takai, Y. Yonemura, H. Minamiue, H. Tagawa, M. Dokiya, H. Inaba, K. Naraya, T. Sasamoto, T. Hashimoto, Solid State Ionics 129 (1–4) (2000) 163.
[19] J. Nowotny, M. Rekas, Journal of the American Ceramic Society 81 (1) (1998) 67.
[20] F.W. Poulsen, Solid State Ionics 129 (1–4) (2000) 145.
[21] K. Yasumoto, N. Mori, J. Mizusaki, H. Tagawa, M. Dokiya, Journal of the Electrochemical Society 148 (1) (2001) A105.
[22] J.H. Kuo, H.U. Anderson, Journal of Solid State Chemistry 87 (1990) 55.
[23] J. Kennedy, R.C. Eberhardt, Proceedings of the IEEE International Conference in Neural Networks, Perth, Australia, 1995, p. 1942.
[24] R. Mendes, J. Kennedy, J. Neves, IEEE Transaction on Evolutionary Computation 8 (3) (2004) 204.
[25] M. Clerc, J. Kennedy, IEEE Transaction on Evolutionary Computation 6 (1) (2002) 58.
[26] B. Carnes, N. Djilali, Journal of Power Sources 144 (1) (2005) 83.
[27] M.B. Giles, N.A. Pierce, Turbulence and Combustion 65 (2000) 393.
[28] F.C. Larché, J.W. Cahn, Acta Metallurgica 30 (10) (1982) 1835.
[29] J. Mizusaki, Y. Yonemura, H. Kamata, K. Ohyama, N. Mori, H. Takai, H. Tagawa, M. Dokiya, K. Naraya, T. Sasamoto, H. Inaba, T. Hashimoto, Solid State Ionics 132 (3–4) (2000) 167.